Since January 2020 Elsevier has created a COVID-19 resource centre with free information in English and Mandarin on the novel coronavirus COVID-19. The COVID-19 resource centre is hosted on Elsevier Connect, the company's public news and information website.

Phytomedicine 108 (2023) 154545

Contents lists available at ScienceDirect

Phytomedicine

journal homepage: www.elsevier.com/locate/phymed

Original Article

Xuanfei Baidu formula alleviates impaired mitochondrial dynamics and activated NLRP3 inflammasome by repressing NF-κB and MAPK pathways in LPS-induced ALI and inflammation models

Zhenhao Li [a,b,*], Haitao Pan [b], Jihong Yang [a,b], Dongjie Chen [b], Yu Wang [c], Han Zhang [a,d,**], Yiyu Cheng [a,c]

[a] College of Pharmaceutical Sciences, Zhejiang University, Hangzhou 310058, China
[b] BoYu Intelligent Health Innovation Laboratory, Hangzhou 311121, China
[c] State Key Laboratory of Component-based Chinese Medicine, Tianjin 301617, China
[d] Institute of Traditional Chinese Medicine, Tianjin University of Traditional Chinese Medicine, Tianjin 301617, China

ARTICLE INFO

Keywords:
Xuanfei Baidu Formula
Mitochondrial dynamics
NLRP3 inflammasome
COVID-19
Inflammation

ABSTRACT

Background: Xuanfei Baidu Formula (XBF) is an effective traditional Chinese medicine (TCM) remedy for treating coronavirus disease 2019 (COVID-19) in China. This herbal medicine has shown effects in reducing clinical symptoms and shortening the average length of hospital stay for COVID-19 patients. Previous studies have demonstrated that XBF alleviates acute lung injury (ALI) by regulating macrophage-mediated immune inflammation, but the mechanisms of action remain elusive.

Purpose: This study aimed to evaluate the lung-protective and anti-inflammatory effects of XBF and its underlying mechanisms.

Methods: Here, XBF's effects were investigated in an ALI mouse model induced by inhalation of atomized lipopolysaccharide (LPS). Besides, the LPS-induced inflammation model in RAW264.7 cells was used to clarify the underlying mechanisms of XBF against ALI.

Results: Our results showed that XBF treatment alleviated LPS-induced lung injury, as evidenced by reduced histopathological changes, pulmonary alveoli permeability, fibrosis, and apoptosis in the lung tissues. In addition, inflammation was alleviated as shown by decreased levels of tumor necrosis factor (TNF)-α, interleukin (IL)-6, IL-1β in serum and bronchoalveolar lavage fluid (BALF), and reduced white blood cell (WBC) count in BALF. Furthermore, consistent with the *in vivo* assay, XBF inhibited LPS-induced inflammatory cytokines release and pro-inflammatory polarization in RAW264.7 cells. Mechanistically, XBF increased mitochondrial fusion by upregulating Mfn1 and attenuated NLRP3 inflammasome activation by repressing Casp11, respectively, to inhibit NF-κB and MAPK pathways, thus repressing pro-inflammatory macrophage polarization.

Conclusion: In this study, we demonstrate that XBF exerts anti-ALI and -inflammatory effects by recovering mitochondrial dynamics and reducing inflammasome activation, providing a biological illustration of the clinical efficacy of XBF in treating COVID-19 patients.

Introduction

Severe acute respiratory syndrome coronavirus 2 (SARS-Cov-2) caused an outbreak of atypical pneumonia at the end of 2019 and led to a global pandemic with 456 million positive cases, including 6 million deaths by March 2022. This virus is a new pathogen with strong infectiousness and fast transmission speed, which has caused a significant impact on human security and social stability (Chan et al., 2020; Wang et al., 2020a). Furthermore, clinical studies have shown that SARS-Cov-2 infection (namely coronavirus disease 2019, COVID-19) causes severe respiratory illnesses, such as acute lung injury (ALI) and systemic inflammatory response (Chen et al., 2020; Coronaviridae Study Group of the International Committee on Taxonomy of 2020; Musa et al., 2021). Indeed, inflammatory responses from infected cells may

* Corresponding author at: College of Pharmaceutical Sciences, Zhejiang University, Hangzhou 310058, China.
** Corresponding author at: Institute of Traditional Chinese Medicine, Tianjin University of Traditional Chinese Medicine, Tianjin 301617, China.
E-mail addresses: zhenhao@zju.edu.cn (Z. Li), zhanghan@tjutcm.edu.cn (H. Zhang).

https://doi.org/10.1016/j.phymed.2022.154545
Received 29 August 2022; Received in revised form 23 October 2022; Accepted 7 November 2022
Available online 9 November 2022

further promote the infiltration of immune cells into the pulmonary interstitial and pulmonary alveoli, causing overproduction of pro-inflammatory cytokines, known as cytokine storm, and finally, leading to severe lung damage and multi-organ dysfunction (Grant et al., 2021; Jose and Manuel, 2020; Li et al., 2022). So far, with the continuous research and development of anti-COVID-19 drugs, several specific drugs or vaccines are clinically available to treat the COVID-19 infection, such as Paxlovid, Sotrovimab, Tocilizumab, and Myancopharm (Drozdzal et al., 2021). However, side effects from vaccines or drugs are inevitable, causing failure in combating the COVID-19-induced cytokine storm, a crucial reason for the high mortality of severe patients and COVID-19-related sequelae (LaVergne et al., 2021). Therefore, the discovery and development of effective agents for treating COVID-19-induced cytokine storms are urgently needed.

Macrophage-mediated inflammation plays a critical role in the pathogenesis of ALI (Kumar, 2020). Resting macrophages can differentiate into pro-inflammatory M1 and anti-inflammatory M2 macrophages (Sica et al., 2015), functioning as primary regulators of inflammation induction and resolution (Ross et al., 2021). Rest macrophages undergo pro-inflammation polarization in response to mild bacteria and virus infections. Polarized macrophages secrete pro-inflammatory mediators such as tumor necrosis factor (TNF)-α, interleukin (IL)-6, and IL-1β, thus inducing host immune defense to clear bacteria and viruses. However, severe bacteria and virus infections cause macrophage overactivation and induce cytokine storms. Recent studies have also found that the uptake of SARS-Cov-2 by M1 macrophages facilitates the release of nucleic acids from virus particles and accelerates the viral replication process (Lv et al., 2021; Sefik et al., 2022). Therefore, targeting pro-inflammatory macrophage polarization is an attractive strategy for treating COVID-19.

Several pre-clinical and clinical trials have confirmed the benefit of traditional Chinese medicine (TCM) in treating COVID-19 (Wang et al., 2020b; Wang and Yang, 2021). Xuanfei Baidu Formula (XBF) was designed by Academician Boli Zhang and Professor Qingquan Liu and approved as a first-line TCM formula for treating COVID-19 patients in China. A pilot randomized clinical trial suggested that XBF showed advantages in compromising symptomatic transition from moderate to severe disease states and improved COVID-19 patients' clinical symptoms, including fever, cough, fatigue, and appetite (Pan et al., 2020). Immunological detection also found that XBF combined with conventional therapy could alleviate lung inflammation with the number of lymphocytes and white blood cells increased (Li et al., 2021b; Xiong et al., 2020). Recently, several studies reported that XBF reduced ALI by regulating the NF-κB-mediated cytokine production and PD-1/IL17A-mediated neutrophils and macrophages infiltration in lung tissue (Li et al., 2021b; Wang et al., 2022b; Zhao et al., 2021b). However, the detailed mechanisms of XBF in anti-inflammatory effects are not fully understood.

This work detected XBF's effects on the lipopolysaccharide (LPS)-induced inflammation and lung injury mice model. XBF significantly reduced the infiltration of macrophages in the lung tissue, showing an excellent anti-inflammatory effect. We employed the *in vitro* LPS-induced macrophage inflammation model to further reveal the mechanism of action. XBF inhibited LPS-induced pro-inflammatory M1 polarization by repressing MAPK and NF-κB pathways.

Materials and methods

Cell culture and reagents

The mice mononuclear macrophage RAW264.7 cells were purchased from American Type Culture Collection (ATCC, USA). Cells were cultured with Dulbecco's Modified Eagle's Medium/Nutrient Mixture F-12 (DMEM/F12, Gibco, USA) supplemented with 5% fetal bovine serum (FBS, Gemini, USA) and 1% penicillin-streptomycin (Gibco, USA), and maintained in a 5% CO_2 incubator at 37 °C. SR-18292 was obtained from MedChemExpress Technology (USA, Cat: HY-101491). XBF extract was provided by State Key Laboratory of Component-based Chinese Medicine (Tianjin) and dissolved in DMEM/F12 at 10 mg/ml as the stock solution, which was then filtered using a 0.22-μm membrane for the following experiments. We provided detail of XBF chemical composition analysis in Supplementary file 1. LipoFiter 3.0^{TM} Liposomal Transfection reagents were purchased from Hanbio Biotechnology (Shanghai, China).

Cell viability assays

In each well of a 96-well plate, 1×10^4 RAW264.7 cells were seeded with 200 μl serum-containing DMEM/F12 medium. Cells were used for testing when they reached 40-50% confluence. 0, 0.25, 0.5, 0.75, 1, 2, 3 and 4 mg/ml XBF was incubated with cells for 24 h to evaluate cytotoxicity. CCK-8 Kit (Beyotime Biotechnology, China, Cat: C0038) was used to measure cell viability. The viability percentage was calculated using the formula below: $(A_{sample}\text{-}A_{blank})/(A_{control}\text{-}A_{blank}) \times 100\%$, where A is the absorbance measured by a microplate reader (Molecular Devices Instrument Inc., USA) under 490 nm.

Plasmid transfection

Cells were seeded in 6-well plates for 24 h. Plasmid DNA and LipoFiter 3.0^{TM} reagent were separately diluted in DMEM/F12 without serum, mixed, and incubated for 20 min. Next, the combination of plasmid and reagent was added to each well, mixed gently, and set in a CO_2 incubator at 37 °C for 12 h. Then, the fresh DMEM/F12 containing 5% FBS was replaced and continued with incubation for 12 h. To determine the expression of *Mfn1* or *Casp11* after transfection, we performed quantitative real-time PCR (qRT-PCR) to detect *Mfn1* or *Casp11* mRNA expression levels.

RNA isolation and qRT-PCR

EASYspin reagent kit (Biomed Biotech, China, Cat: RA105-01) was used to isolate total RNA according to the manufacturer's protocol. Total RNA quality and quantity were analyzed using a NanoDrop^{TM} one spectrophotometer (Thermo Scientific, Grand Island, NY, USA). An iScript Reverse transcription supermix (Vazyme Biotech, China) was used to synthesize first-strand cDNA from 1 μg total RNA. qRT-PCR analysis was performed using Faststart Essential DNA Green Master (Roche, Basel, Swit, Cat: 06402712001) on LightCycler96 Real-Time PCR system (Roche). Primers were designed with Primer3Plus software (Cambridge, USA). GAPDH was used as the reference gene. The relative expression of mRNA was calculated by following the previous literature (Na et al., 2017). qRT-PCR primer sequences are shown in Supplementary Table 1.

Western blotting

Polyclonal peroxisome proliferator-activated receptor γ coactivator 1α (PGC-1α) antibody was purchased from Affinity Biosciences (Jiangsu, China). Polyclonal Mfn1 antibody was purchased from ZEN-Biosciences (Chengdu, Sichuan, China). Polyclonal p-IκKα (Thr23), p-NF-κB p65 (Ser529) antibodies, and Monoclonal Mfn2, IκKα, NF-κB p65 antibodies were purchased from Abways Technology (Shanghai, China). Polyclonal p-IκBα (Ser36), p-P38 (Thr180/Tyr182), p-Erk1/2 (Thr202/185), IκBα, P38, Erk1/2, iNOS, and β-Actin antibodies were purchased from Diag Bio-technology (Hangzhou, China). Cells were lysed in ice-cold RIPA buffer (Beyotime Biotechnology, China, Cat: P0013K) supplemented with protease inhibitors, and protein concentrations were measured by bicinchoninic acid (BCA) protein assay kit (Pierce, Rockford, USA, Cat: 23228). An equal amount of total protein (30 μg) was separated by SDS–PAGE and transferred to PVDF (polyvinylidene fluoride) membrane (Millipore, USA). After blocking with 5% nonfat milk in 1 × TBST at room temperature (RT) for 1 h, membranes were incubated with the

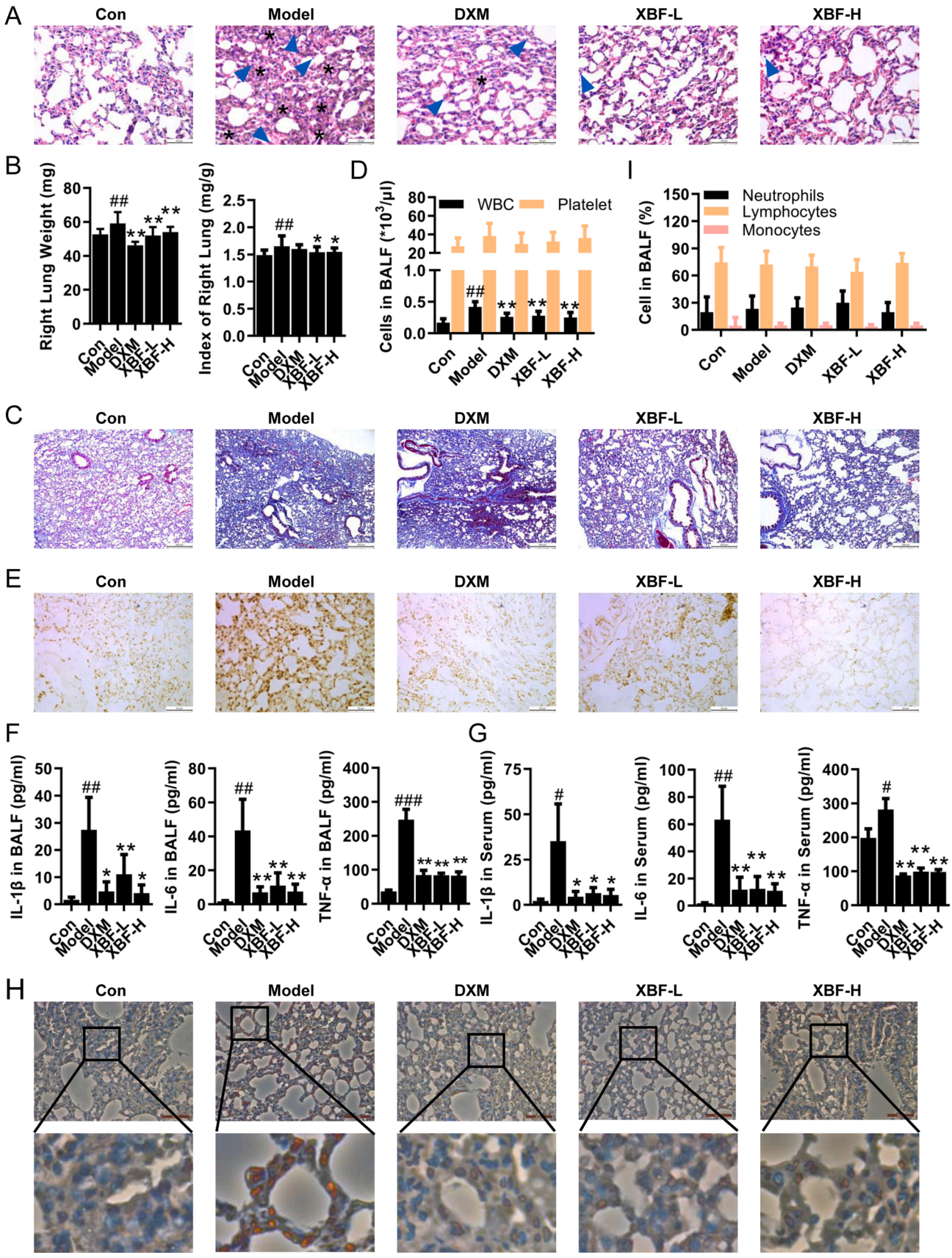

(caption on next page)

Fig. 1. XBF attenuated LPS-induced acute lung injury *in vivo*. (A) Histological analysis of lung tissue sections was stained by hematoxylin and eosin (H&E staining, the asterisks indicate alveolar collapse and arrows indicate inflammatory infiltration) (400 ×). Scale bar = 50 μm, $n = 6$. (B) Right lung weight and lung index of each group. (C) Fibrosis analysis of lung tissue sections was evaluated by Masson's trichrome staining (100 ×). Scale bar = 200 μm, $n = 6$. (D) The counts of WBC and platelet in BALF were counted using a hemocytometer. (E) Cell apoptosis was detected by TUNEL staining (400 ×). Scale bar = 50 μm, $n = 6$. (F-G) The expression of IL-1β, IL-6, and TNF-α in BALF and serum ($n = 6$). (H) The expression of macrophage markers F4/80 was determined by immunohistochemical (IHC) staining in lung tissues (400 ×). Scale bar = 50 μm, $n = 6$. (I) The percentage of neutrophils, lymphocytes, and monocytes in BALF was counted using a hemocytometer. Data are presented as the mean ± SE from 15 lung tissue samples of each group. $^{\#}p < 0.05$; $^{\#\#}p < 0.01$; $^{\#\#\#}p < 0.001$ compared with con group; $^{*}p < 0.05$; $^{**}p < 0.01$ compared with model group.

primary antibody (Sources and Dilutions of primary antibodies are shown in Supplementary Table 2) overnight at 4 °C. The membranes were washed with TBST and incubated with a secondary antibody for 1 h at RT. Then signals were captured using western lightning Plus-ECL (PerkinElmer, USA, Cat: 203-19031) and iBright 1500 imaging System (Invitrogen, USA). ImageJ 1.41 software (Bethesda, USA) was used for western blot quantitative analysis. Original images of all western blot data were provided in Supplementary file 2.

Evaluation of mitochondrial membrane potential (ΔΨm) and Mitochondrial tracking

RAW264.7 cells were seeded in 6-well plates (2×10^4 cells per well) and incubated overnight. Inflammation markers, such as IL-6 and IL-1β, were significantly upregulated by 12 h LPS stimulation and maintained at a high level during 24-72 h LPS stimulation (Liu et al., 2019). Considering that, LPS (0.1 μg/ml) stimulation was first conducted for 12 h to induce inflammation model. Then, the XBF was added and incubated for another 24 h to investigate XBF's effects when inflammation factors were maintained at high levels. Next, the cells were harvested and washed with PBS. Then cells were stained with JC-1 to evaluate mitochondrial membrane potential by following the manufacturer's instructions (Beyotime Biotechnology, Cat: C2006). After the same treating procedures with the above ΔΨm experiment, cells were washed with ice-cold PBS and incubated with Mito-Tracker probes (100 nM) for 30 min at RT in the dark. Both experiments' fluorescence intensities were captured using ImageXpress Micro Confocal imaging system (BD Pharmingen, USA).

Lactic acid (LA) and ATP measurements

LA and ATP levels were measured using LA (Cat: BC2235) or ATP (Cat: S0026) assay kit (Solarbio life sciences, China) using the corresponding manufacturer's instructions.

LPS-induced ALI model

Eight-to-ten-week adult male ICR mice were purchased from Hangzhou Medical College and maintained in the specific-pathogen-free (SPF) condition after breeding for several days. All methods applied in this study were carried out in accordance with the 'Principles of Laboratory Animal Care of National Institutes of Health' and 'guidelines of laboratory animal care committee of Xi'an Jiaotong University' (Supplementary file 3). Furthermore, all procedures are in line with the Animal Welfare Act Regulations. The treatment of animals was the same as in the previous paper (Fang et al., 2017). Briefly, the mice ($n = 80$) were randomly divided into a control group ($n = 16$) and a model group ($n = 64$). The model group was administered with the inhaled atomized-LPS (2.5 mg/ml in saline) to induce ALI. After LPS (Sigma, Saint Louis, Missouri, Cat: L2880) administration for 3 d, the mice ($n = 64$) were randomly divided by weight into four groups: LPS group, LPS plus high XBF concentration treatment (4.32 g/kg) group, LPS plus low XBF concentration treatment (2.16 g/kg) group, and LPS plus Dexamethasone treatment (DXM, Aladdin Biotechnology, Shanghai, China, Cat: D137736, 0.4 mg/kg) group ($n = 16$ per group). All drugs were treated with gavage per day, while LPS and control groups were treated with saline. After XBF or DXM administration for 14 d, the animals were euthanized. For further analyses, we collected the bronchoalveolar lavage fluid (BALF), blood, and lung tissues.

BALF collection and analysis

After the mice were euthanized, the thorax was opened, and ice-cold PBS (0.3 ml) was instilled into the lung and withdrawn via tracheal incision three times (Pastva et al., 2004). Next, the recovered BALF was centrifuged (400 g, 20 min) at 4 °C. Then, the cell-free supernatants were used for cytokine measurements by ELISA. The cell pellet was suspended in 1 ml PBS used for cell proportion measurements by a fully automatic blood analyzer (XT-2000i, Sysmex).

Enzyme-linked immunosorbent assay

ELISA kits were purchased from Jiangsu Meimian Industrial Co., Ltd for measuring the levels of IL-1β (Cat: MM-0040M1), IL-6 (Cat: MM-0163M1), and TNF-α (Cat: MM-0132M1) in BALF, serum, and cell culture medium. Total protein concentrations were determined using the BCA protein assay kit (Pierce, USA, Cat: 23228).

Lung histological examination

The harvested lung tissues were fixed in 4% paraformaldehyde, embedded in paraffin, and cut into 4-μm sections. Then, the sections were stained with hematoxylin and eosin (H&E) according to the previous description (Na et al., 2017). Finally, morphological changes in lung tissues were recorded by a microscope (DM4000, Leica Biosystems).

Pulmonary fibrosis examination

Lung sections were stained using the Masson kit (Solarbio life sciences, Cat: G1340). The blue or green signal indicated positive staining for collagen, and the red indicated positive staining for muscle fibers. Images were captured by a microscope DM4000 (Leica Biosystems).

TUNEL staining

Lung tissue samples were harvested and fixed in 10% formalin for 24 h. Fixed lung tissues were embedded in paraffin, and 5-μm sections were used for TUNEL staining using the TUNEL assay kit (Beyotime Biotechnology, Cat: C1098).

Immunohistochemistry

Formalin-fixed lung tissues were embedded and deparaffinized. Hydrogen peroxide (3%) and 2% BSA were used for 30 min-blocking. The slides were incubated overnight at 4 °C with F4/80 primary antibodies (Affinity Biosciences, Cat: DF2789). Then, the slides were incubated with anti-goat IgG secondary antibody for 60 min at RT. After washing, slides were stained with 3,3-diaminobenzidine (DAB), washed and counterstained with hematoxylin, dehydrated, and then mounted with a coverslip. DM4000 microscope was used to capture images.

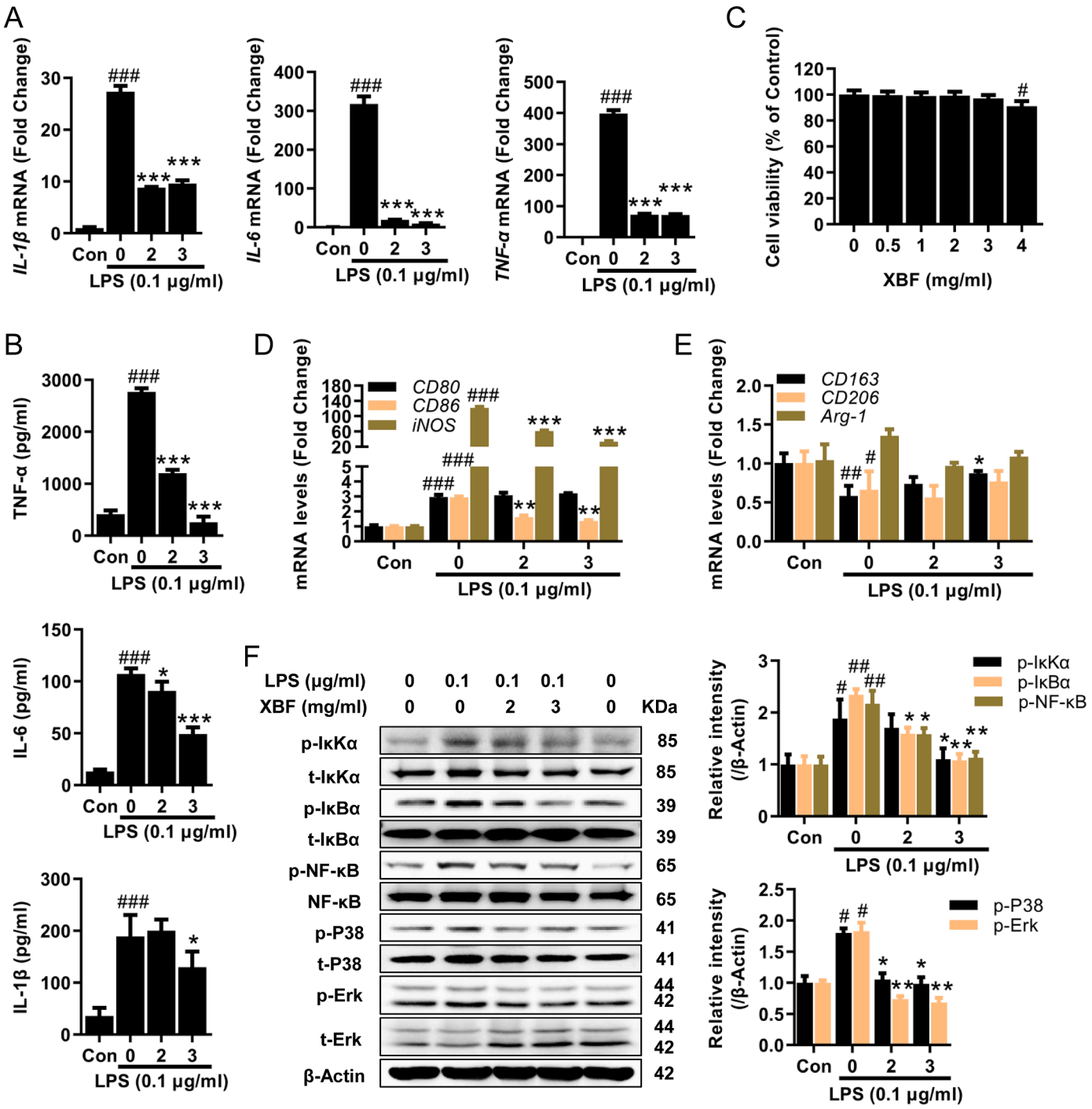

Fig. 2. XBF attenuated LPS-induced inflammation in RAW264.7 cells. (A) qRT-PCR determination of the mRNA expression of *IL-1β, IL-6,* and *TNF-α* in RAW264.7 cells upon treatment with XBF (2 and 3 mg/ml) for 24 h. (B) Concentration of IL-1β, IL-6 and TNF-α in cell culture medium was examined by ELISA assay, and data presented were normalized by the concentration of protein lysates. (C) RAW264.7 cells were treated with XBF (0.5, 1, 2, 3 and 4 mg/ml) for 24 h. Cell viability was measured by the CCK-8 assay. (D-E) qRT-PCR determination of the mRNA expression of *CD80, CD86, iNOS, CD163, CD206*, and *Arg-1* in RAW264.7 cells upon treatment with XBF (2 and 3 mg/ml) for 24 h. (F) RAW264.7 cells were treated with XBF (2 and 3 mg/ml) for 24 h, the expression of both phosphorylated and total IκKα, IκBα, NF-κB, P38, and Erk were determined by western blotting. β-Actin was used as an internal control. Data are presented as the mean ± SE from three independent experiments. $^{\#}p < 0.05$; $^{\#\#}p < 0.01$; $^{\#\#\#}p < 0.001$ compared with untreated cells; $^{*}p < 0.05$; $^{**}p < 0.01$; $^{***}p < 0.001$ compared with LPS-treated cells.

Statistical analysis

All data are expressed as mean ± standard error (SE) of at least three independent experiments. The student *t*-test was used for comparing two conditions, and one-way analysis of variance (ANOVA) with Tukey's test was used for multiple comparisons. All analyses were performed using GraphPad Prism 5.0 (Graphpad Software, Inc., USA) with a *p*-value less than 0.05 considered statistically significant.

Results

XBF attenuated LPS-induced ALI and inflammation in vivo

To evaluate the therapeutic action of XBF against endotoxin-induced

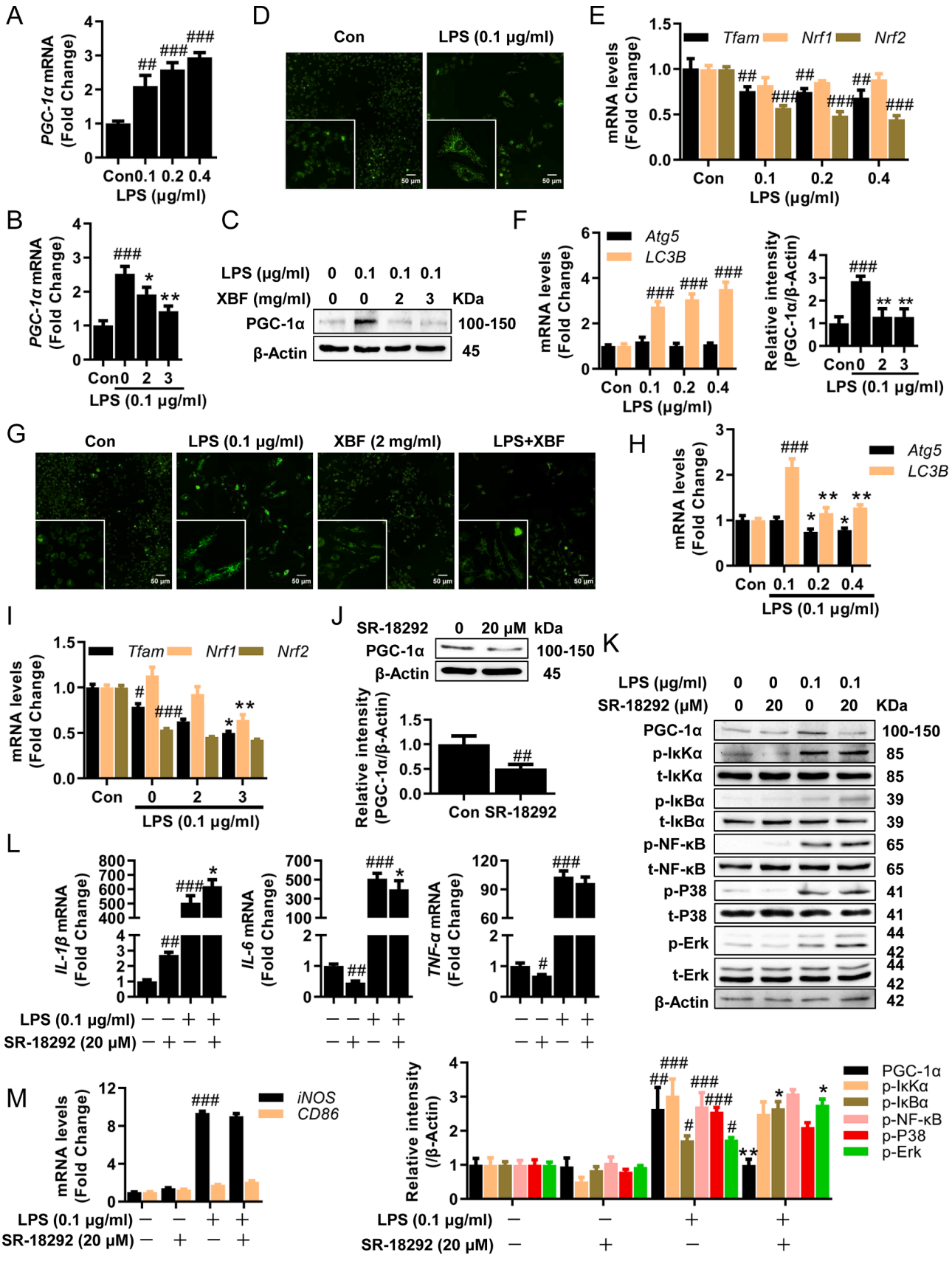

(caption on next page)

Fig. 3. XBF inhibited IL-6 expression by inhibiting mitochondrial biosynthesis in RAW264.7 cells. (A) qRT-PCR determination of the mRNA expression of *PGC-1α* in RAW264.7 cells upon treatment with LPS at indicated concentrations for 24 h. (B) Quantification of the mRNA of *PGC-1α* in RAW264.7 cells upon treatment with XBF (2 and 3 mg/ml) for 24 h. (C) Western blotting analysis of the PGC-1α protein in RAW264.7 cells upon XBF (2 and 3 mg/ml) treatment for 24 h. β-Actin was used as an internal control. (D) Increased mitochondrial biosynthesis upon treatment with LPS in RAW264.7 cells as determined by Mito-Tracker Green staining. Representative fluorescence microscopy images are shown (400 ×). Scale bar = 50 μm. (E-F) qRT-PCR determination of the mRNA expression of *Tfam, Nrf1, Nrf2* (E), *Atg5, LC3B* (F) in RAW264.7 cells upon treatment with LPS at indicated concentrations for 24 h. (G) Inhibition of mitochondrial biosynthesis upon treatment with XBF (2 mg/ml) for 24 h in RAW264.7 cells as determined by Mito-Tracker Green staining. Representative fluorescence microscopy images are shown (400 ×). Scale bar = 50 μm. (H-I) Quantification of the mRNA of *Atg5, LC3B* (h), *Tfam, Nrf1, Nrf2* (i) in RAW264.7 cells upon treatment with XBF (2 and 3 mg/ml) for 24 h. (J) Western blotting analysis of PGC-1α proteins in RAW264.7 cells upon SR-18292 (20 μM) treatment for 24 h. β-Actin was used as an internal control. (K) RAW264.7 cells were co-treated with LPS and SR-18292 for 24 h, the expression of PGC-1α and both phosphorylated and total IκKα, IκBα, NF-κB, P38, and Erk were determined by western blotting. β-Actin was used as an internal control. (L-M) RAW264.7 cells were co-treated with LPS and SR-18292 for 24 h, the expression of *IL-1β, IL-6, TNF-α* (l) and *iNOS, CD86* (m) mRNA were determined by qRT-PCR. Data are presented as the mean ± SE from three independent experiments. $^{\#}p < 0.05$; $^{\#\#}p < 0.01$; $^{\#\#\#}p < 0.001$ compared with untreated cells; $^{*}p < 0.05$; $^{**}p < 0.01$; $^{***}p < 0.001$ compared with LPS-treated cells.

pneumonia, ALI was induced in mice with LPS exposure. Lung tissues, BALF, and serum were collected for evaluation. As shown in Fig. 1A, B, XBF treatment ameliorated LPS-induced interstitial edema, infiltration of inflammatory cells, thickening of alveolar walls, and alveolar collapse. Masson staining further showed that XBF treatment attenuated LPS-induced collagen deposition in lung tissues (Fig. 1C). In addition, the pulmonary alveoli permeability was evaluated based on cell counts in BALF. As shown in Fig. 1D, treatment with high concentration XBF exhibited comparable effects as DXM on decreasing the WBC and platelet count, suggesting that XBF compromised LPS-induced inflammation.

Cytokine-mediated inflammatory cell death is observed during bacterial or virus-associated ALI (Karki et al., 2021; Kumar, 2020). Consistently, LPS inhalation significantly increased the apoptotic cell proportion in lung tissues as characterized by TUNEL staining, while XBF and DXM significantly reduced LPS-induced apoptotic cells (Fig. 1E). Meanwhile, we observed that pro-inflammatory cytokines IL-1β, IL-6, and TNF-α were elevated by LPS stimulation in the BALF and serum while reduced by either XBF or DXM (Fig. 1F, G). Given that inflammation is an apoptosis-triggering factor (Yang et al., 2015), we analyzed the effect of XBF on the infiltration of inflammation-regulating cells in lung tissues and observed a reduction of F4/80-positive macrophage cells (Fig. 1H). On the other hand, there was no significant change in neutrophils, lymphocytes, and monocytes from BALF upon XBF treatment on LPS-induced ALI mice (Fig. 1I).

These results indicate that XBF inhibits LPS-induced ALI and inflammation *in vivo*, which may be related to macrophage infiltration and macrophage-related regulation.

XBF attenuated LPS-induced pro-inflammatory macrophage polarization through NF-κB and MAPK pathways

To further understand how XBF inhibits inflammation through macrophages, we employed the LPS-induced inflammation model in RAW264.7 macrophage cells. Consistent with the *in vivo* observation mentioned above, XBF treatment dose-dependently decreased IL-1β, IL-6, and TNF-α expression at both mRNA (Fig. 2A) and protein (Fig. 2B) levels with no apparent toxicity (Fig. 2C).

Considering that macrophages can be polarized into pro-inflammatory M1 or anti-inflammation M2 phenotypes (Liu et al., 2014), we further analyzed the effect of XBF on M1 and M2 markers. M1 markers *CD86* and *iNOS* were significantly decreased by XBF (Fig. 2D), while M2 marker *CD163* increased (Fig. 2E), supporting the inhibiting role of XBF in pro-inflammatory polarization.

Previous studies have demonstrated that IκKα/IκBα/NF-κB and MAPK play a vital role in the pro-inflammatory polarization of macrophages (Liu et al., 2020). Therefore, we next examined the effects of XBF on these signaling pathways. As shown in Fig. 2F, XBF significantly reduced LPS-induced phosphorylation of IκKα, IκBα, NF-κB, P38, and Erk. These results suggest that XBF inhibits LPS-induced pro-inflammatory macrophage polarization by inhibiting IκKα/IκBα/NF-κB and MAPK signaling pathways.

XBF reduced PGC-1α expression, leading to mitochondria mass loss but not pro-inflammatory polarization

In addition to pro-inflammation macrophage polarization, we would like to know whether other factors were involved in regulating inflammation upon XBF treatment. Mitochondria have been well recognized as a master regulator of inflammation (Galluzzi et al., 2012). To understand whether XBF regulates mitochondria in inhibiting inflammation, we analyzed XBF's effects on mitochondrial function. LPS significantly upregulated the mitochondria master regulator PGC-1α (Halling and Pilegaard, 2020) expression (Fig. 3A–C) and mitochondrial mass (Fig. 3D). On the other hand, LPS inhibited the expression of *Tfam*, and *Nrf2*, two critical factors for removing damaged mitochondria DNA (Fig. 3E), suggesting that LPS induced the accumulation of damaged mitochondria, which was further supported by the upregulation of autophagy markers LC3B upon LPS treatment in RAW264.7 cells (Fig. 3F). In combating LPS stimulation, XBF partially reversed PGC-1α expression (Fig. 3B, C), mitochondrial mass (Fig. 3G), and autophagy marker LC3B expression (Fig. 3H), but interestingly, XBF treatment did not rescue the downregulated *Tfam* and *Nrf2* expression upon LPS stimulation (Fig. 3I). In addition, XBF significantly downregulated the expression of *Nrf1* (Fig. 3I), though LPS did not affect its expression (Fig. 3E). These results indicate that the main effect of XBF on mitochondria might rely on reducing PGC-1α expression.

SR-18292, a PGC-1α inhibitor (Fig. 3J, K), did not affect IL-1β and TNF-α (Fig. 3L) but decreased IL-6 expression (Fig. 3L). Moreover, SR-18292 did not affect LPS-induced IκK/IκB/NF-κB, P38, Erk activation, and pro-inflammatory polarization (Fig. 3K, M). Given these, XBF reduced PGC-1α expression, which is responsible for compromising mitochondria biosynthesis but not pro-inflammatory polarization.

XBF-induced mitochondrial fusion inhibited M1 phenotype conversion by targeting NF-κB pathway

Since the mitochondria synthesis is not the causal factor in combating inflammation upon XBF treatment, we then investigated mitochondria dynamics, including division, fusion, and cristae remodeling, which have been proposed as the main triggering factors for inflammation (Geto et al., 2020). First, we analyzed the role of mitochondrial dynamics in the anti-inflammatory effect of XBF. LPS-treated cells exhibited a dramatic decrease in mitochondria division/fusion-related genes *Drp1, Fis1, Opa1, Mfn1*, and *Mfn2* (Fig. 4A). Among these, the mitochondria fusion regulator Mfn1 and Mfn2 were significantly and slightly upregulated by XBF, respectively (Fig. 4B, C). In addition, XBF decreased the intensity of JC-1, a fluorescent probe for measuring mitochondria membrane potential ΔΨm (Fig. 4D), which is in line with the XBF's effect on alleviating the impairment of mitochondria dynamics.

The change in mitochondria dynamics, such as mitochondria fusion, could promote the capacity of oxidative phosphorylation (OXPHOS) (Bonnay et al., 2020), which is needed by M2 macrophages (Viola et al., 2019). Following XBF's role in regulating mitochondria dynamics, the

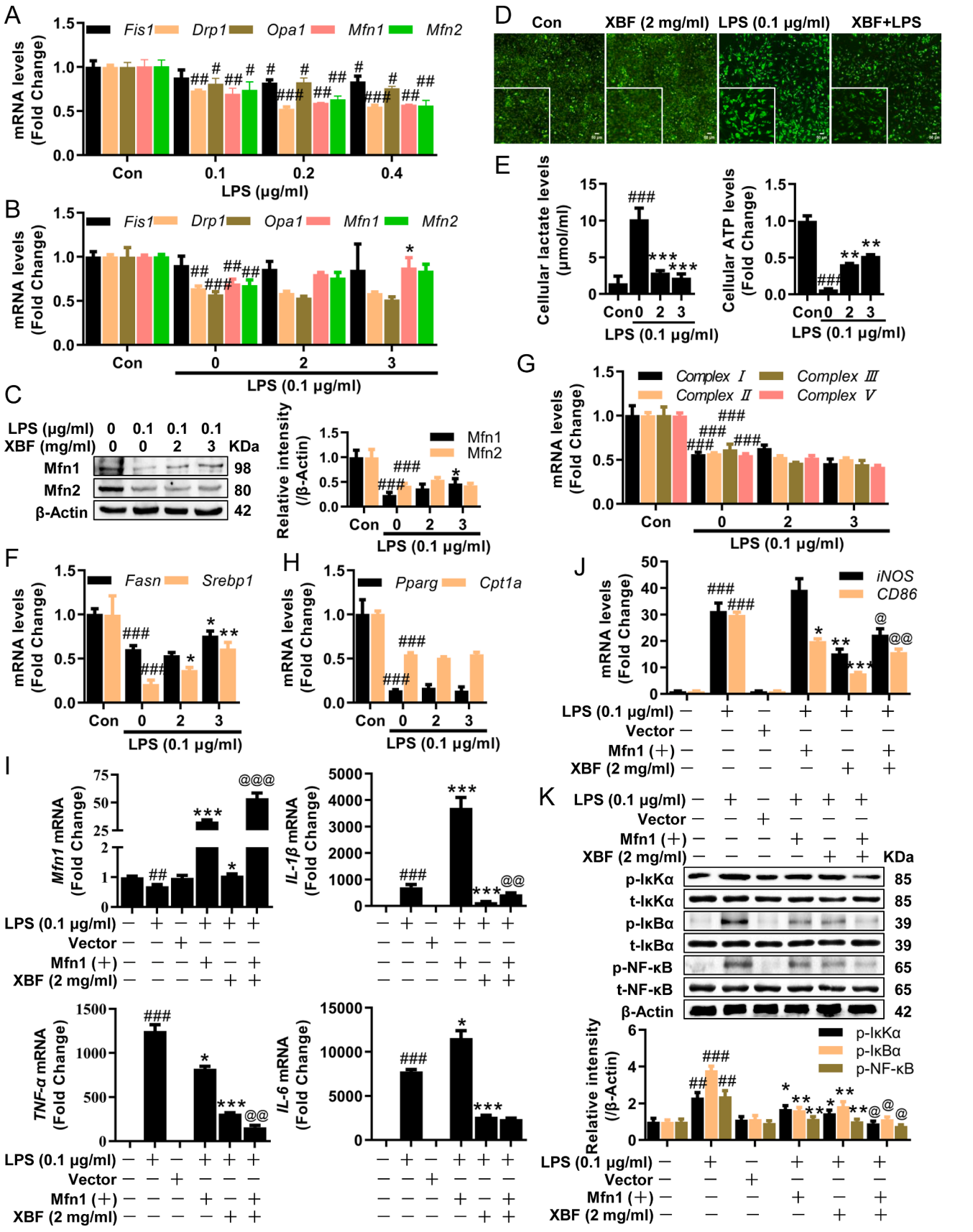

(caption on next page)

Fig. 4. XBF inhibited TNF-α expression by increasing Mfn1-mediated mitochondria fusion in RAW264.7 cells. (A) qRT-PCR determination of the mRNA expression of *Opa1, Mfn1, Mfn2, Drp1,* and *Fis1* in RAW264.7 cells upon treatment with LPS at indicated concentrations for 24 h. (B) qRT-PCR determination of the mRNA expression of *Opa1, Mfn1, Mfn2, Drp1,* and *Fis1* in RAW264.7 cells upon treatment with XBF (2 and 3 mg/ml) for 24 h. (C) Western blotting analysis of Mfn1 and Mfn2 proteins in RAW264.7 cells upon XBF (2 and 3 mg/ml) treatment for 24 h . β-Actin was used as an internal control. (D) Increases of mitochondrial membrane potential upon treatment with XBF (2 mg/ml) for 24 h in RAW264.7 cells as determined by JC-1 staining. Representative fluorescence microscopy images are shown (200 ×). Scale bar = 50 μm. (E) RAW264.7 cells were treated with XBF (2 and 3 mg/ml) for 24 h, the intracellular ATP and lactate levels were measured. (F-H) qRT-PCR determination of the mRNA expression of *Fasn, Srebp1* (f), mitochondrial *complex I, II, III, V* (g), *Pparg, Cpt1a* (h) in RAW264.7 cells upon treatment with XBF (2 and 3 mg/ml) for 24 h. (I-J) RAW264.7 cells were transfected with Mfn1 overexpression plasmid and treated with XBF (2 mg/ml) for 24 h, the expression of *Mfn1, IL-1β, IL-6, TNF-α* (i), and *iNOS, CD86* (j) mRNA were determined by qRT-PCR. (K) RAW264.7 cells were transfected with Mfn1 overexpression plasmid and treated with XBF (2 mg/ml) for 24 h, the expression of both phosphorylated and total IκKα, IκBα, and NF-κB were determined by western blotting. β-Actin was used as an internal control. Data are presented as the mean ± SE from three independent experiments. $^{\#}p < 0.05$; $^{\#\#}p < 0.01$; $^{\#\#\#}p < 0.001$ compared with untreated cells; $^{*}p < 0.05$; $^{**}p < 0.01$; $^{***}p < 0.001$ compared with LPS-treated cells; $^{@}p < 0.05$; $^{@@}p < 0.01$ compared with XBF-treated cells.

drug significantly reduced intracellular pyruvate (Fig. 4E) while increasing ATP production, promoting the metabolic switch from glycolysis to OXPHOS. Particularly, XBF significantly upregulated the expression of fatty acid synthases, including *Fasn* and *Srebp1* (Fig. 4F). The transcriptional levels of electron transport chain (ETC) complex and fatty acid oxidase-related genes, such as *Cpt1a*, and *Pparg*, were unchanged upon XBF treatment in RAW264.7 cells (Fig. 4G, H), suggesting the rate of OXPHOS is not significantly changed.

To examine whether activated Mfn1 mediates inflammation inhibition by XBF in RAW264.7 cells, we co-treated cells with pcDNA3.1-Mfn1 plasmid to overexpress Mfn1. Upon LPS stimulation, Mfn1-overexpression and XBF downregulated TNF-α and M1 macrophage marker CD86 expression (Fig. 4I). Synergistic inhibitory effect on reducing TNF-α but not CD86 was observed by co-treatment (Fig. 4J). Notably, the XBF and Mfn1-overexpression showed a synergistic inhibitory effect inhibiting the above-mentioned pro-inflammatory macrophage polarization pathway, IκK/IκB/NF-κB pathway (Fig. 4K). These results suggest that XBF-induced mitochondrial fusion inhibits M1 phenotype conversion by targeting IκK/IκB/NF-κB pathway in RAW264.7 cells.

XBF inhibited Casp11/NLRP3 inflammasome to target NF-κB and MAPK pathways

Besides mitochondria fusion, we searched for other upstream of NF-κB and MAPK pathways repressed by XBF. Given those critical roles of mitochondria in activating NLRP3 inflammasome (Liu et al., 2018), we analyzed the effect of XBF on inflammasome activation and its effects on NF-κB and MAPK pathways. Inflammasome sensor genes, *Nlrp1, Nlrp3*, and *Nlrc4*, were significantly downregulated by XBF (Fig. 5A). The caspase family is crucial for inflammasome activation (Man et al., 2017). Of note, the expression of Casp11, a non-canonical NLRP3 inflammasome activator (Kayagaki et al., 2011), was downregulated by XBF (Fig. 5B), suggesting that XBF may inhibit IL-1β synthesis and secretion by inhibiting Casp11-dependent NLRP3 inflammasome activation.

Next, we examined the role of Casp11 in XBF inhibiting LPS-induced inflammation. Indeed, we found that overexpression of Casp11 significantly increased the expression of *IL-1β, iNOS*, and *CD86* mRNA (Fig. 5C–E), suggesting that activation of Casp11 promoted M1 polarization in RAW264.7 cells. Furthermore, the overexpression of Casp11 alleviated the inhibitory effect of XBF on M1 marker iNOS at the protein levels (Fig. 5F). However, it did not reverse the inhibitory effect of XBF on *Casp11, IL-1β, iNOS*, and *CD86* mRNA (Fig. 5D, E, G).

Furthermore, we analyzed the effect of Casp11 overexpression on NF-κB and MAPK signaling pathways. As shown in Fig. 5H, consistent with the previous results, XBF significantly inhibited LPS-induced IκKα/IκBα/NF-κB, P38, and Erk activation. At the same time, overexpression of Casp11 effectively reversed the inhibitory effects of XBF on IκKα/IκBα/NF-κB, P38, and Erk. These results suggest that Casp11 inhibition is responsible for XBF-inhibited pro-inflammatory response in RAW264.7 cells.

Discussion

TCM has been established for thousands of years to treat diseases (Li et al., 2021a). According to TCM theory, the pathological characteristics of COVID-19 infection are summarized as "dampness, heat, toxin, deficiency, and stasis" (Lyu et al., 2021). The XBF comprises 13 medicinal herbs and natural materials (Wang et al., 2020b). Clinical trials prove that XBF can prevent the transition from mild to severe symptoms (Xiong et al., 2020; Zhao et al., 2021a). However, the underlying mechanism by which XBF improves clinical symptoms in COVID-19 patients remains unknown.

Furthermore, although several studies have recently found that XBF reduces ALI by regulating macrophage-mediated immune inflammation *in vitro* or *in vivo* (Li et al., 2021b; Xiong et al., 2020), the exact mechanisms are still unclear. In the present study, we used the LPS-induced ALI mouse model and *in vitro* inflammation model to explore the mechanisms of XBF against ALI. As summarized in Fig. 6, our results indicated that XBF suppressed LPS induced-inflammatory response by correcting impaired mitochondrial dynamics and NLRP3 inflammasome activation, thus compromising NF-κB and MAPK pathways to inhibit pro-inflammatory cytokines polarization in RAW264.7 macrophage cells. Unfortunately, we have yet to fully illustrate the active constituents of XBF due to its complex chemical components. The UPLC-Q-TOF-MS/MS was used to analyze the tissue distribution of Xuanfei Baidu granules in rats, and nine components were detected in the lung tissue (Wang et al., 2022a). In addition, we found that five of the above nine components (emodin, verbenalin, amygdalin, naringenin, naringin) could inhibit TNF-α, IL-1β, or IL-6 in the LPS-induced macrophage inflammation model. Therefore, we speculated that these constituents entering the lung tissue might be the active constituents of XBF. However, more studies are needed to elucidate the active constituents of XBF.

Numerous studies have revealed that mitochondria act as an important intracellular signal platform for inflammatory responses by producing reactive oxygen species (ROS) (Meyer et al., 2018). In contrast, increased mitochondrial biogenesis contributes to the inflammation resolution (Fontecha-Barriuso et al., 2019; Jehn et al., 2021). Therefore, the role of mitochondrial biogenesis in inflammatory response remains controversial. Excessive and uncontrolled production of ROS leads to mitochondrial and tissue damage (Andrieux et al., 2021). Zhong et al. (2018) also reported that inhibition of mtDNA synthesis by TFAM knockout significantly reversed NLRP3-induced caspase-1 activation and IL-1β processing and inhibition of mtDNA synthesis abrogated NLRP3 inflammasome activation (Xian et al., 2021). In line with our results, LPS induces mitochondrial biosynthesis and inhibits mtDNA synthesis and replication, which leads to excessive accumulation of damaged mitochondria and induces inflammation response (Chung et al., 2019). It is noteworthy that XBF not only reduces the accumulation of damaged mitochondria by inhibiting PGC-1α but also further inhibits mtDNA synthesis and replication, suggesting that XBF inhibits mitochondria-mediated inflammation upon acting on multiple targets. In addition, we found that XBF inhibited IL-6 activation by inhibiting PGC-1α, and the results were further verified by co-treatment with LPS

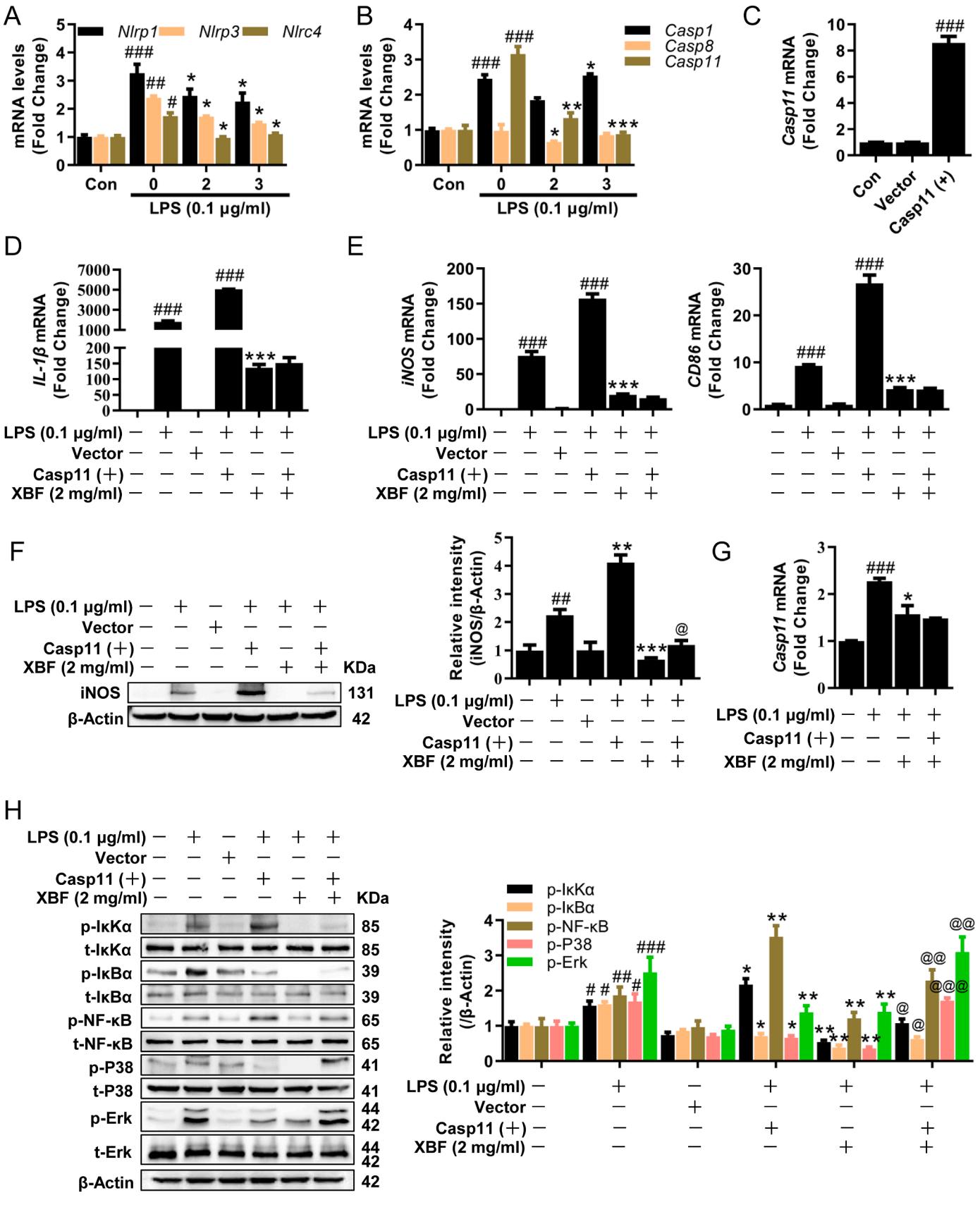

(caption on next page)

Fig. 5. XBF inhibited IL-1β expression by inhibiting Casp11/NLRP3 inflammasome signaling pathway in RAW264.7 cells. (A-B) qRT-PCR determination of the mRNA expression of *Nlrp1, Nlrp3, Nlrc4* (A) and *Casp1, Casp8, Casp11* (B) in RAW264.7 cells upon treatment with XBF (2 and 3 mg/ml) for 24 h. (C) RAW264.7 cells were transfected with Casp11 overexpression plasmid for 6 h, the expression of *Casp11* mRNA were determined by qRT-PCR. (D-E) RAW264.7 cells were transfected with Casp11 overexpression plasmid and treated with XBF (2 mg/ml) for 24 h, the expression of *IL-1β* (d), *iNOS, CD86* (e) mRNA were determined by qRT-PCR. (F) RAW264.7 cells were transfected with Casp11 overexpression plasmid and treated with XBF (2 mg/ml) for 24 h, the expression of iNOS was determined by western blotting. β-Actin was used as an internal control. (G) RAW264.7 cells were transfected with Casp11 overexpression plasmid and treated with XBF (2 mg/ml) for 24 h, the expression of *Casp11* mRNA was determined by qRT-PCR. (H) RAW264.7 cells were transfected with Casp11 overexpression plasmid and treated with XBF (2 mg/ml) for 24 h, the expression of phosphorylated and total IκKα, IκBα, NF-κB, P38, and Erk were determined by western blotting. β-Actin was used as an internal control. Data are presented as the mean ± SE from three independent experiments. $^{\#}p < 0.05$; $^{\#\#}p < 0.01$; $^{\#\#\#}p < 0.001$ compared with untreated cells; $^{*}p < 0.05$; $^{**}p < 0.01$; $^{***}p < 0.001$ compared with LPS-treated cells; $^{@}p < 0.05$; $^{@@}p < 0.01$; $^{@@@}p < 0.001$ compared with XBF-treated cells.

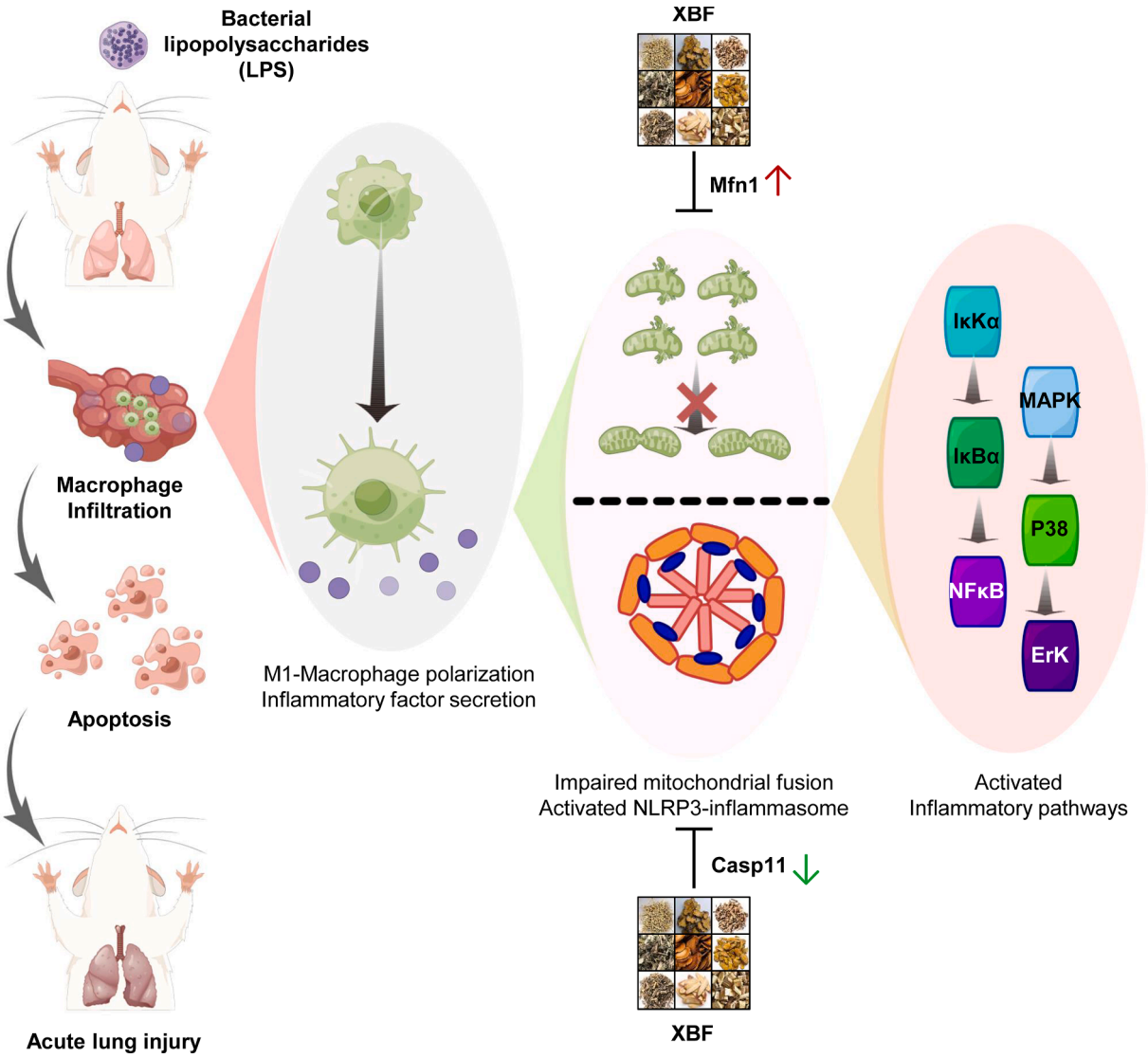

Fig. 6. The protective effect of XBF on LPS-induced acute lung injury and the underlying mechanisms. XBF treatment significantly protected LPS-induced ALI by inhibiting inflammation and apoptosis of lung epithelial cells, which was mediated by the inhibition of mitochondrial biosynthesis, activation of Mfn1-mediated mitochondria fusion, and inhibition of Casp11-dependent non-classical inflammatory pathways.

and SR-18292. However, the effect is independent of the classical inflammation pathway and macrophage polarization. In addition to SR18292, BAY87-2243, a HIF-1 α inhibitor, could affect the mitochondria biogenesis (Saki and Prakash, 2017). Thus, we would like to investigate other vital proteins relevant to mitochondria biogenesis and whether they are involved in regulating XBF's effects.

Interestingly, Rowe et al. (2014) reported that PGC-1α induced phosphoprotein1 (SPP1) secretion in C2C12 myotubes, which activated macrophages to express IL-6, but not TNF-α and IL-1β. Shih et al. also found that low molecular weight fucoidan and high stability fucoxanthin attenuates NAFLD-induced IL-6 and IFN-γ secretion along with SIRT-PGC-1α pathway inhibition (Shih et al., 2021). Therefore, the detailed mechanism of XBF inhibiting IL-6 activation by inhibiting PGC-1α needs to be further studied.

In addition to biogenesis, mitochondrial quality is mainly regulated by dynamics, including fusion and division, which are regulated by multiple proteins and enzymes, as exemplified with Drp1 and Fis1 in the mitochondrial division, Mfn1 and Mfn2 in the mitochondrial fusion (Otera et al., 2013). The interplay of fission and fusion confers widespread benefits on mitochondria. For example, efficient transport and

oxidative phosphorylation increased the mitochondrial mass's homogenization and facilitated the redistribution of mtDNA between damaged and healthy mitochondrial (Chan, 2020). Yu et al. (2020) reported that disruption of mitochondrial dynamics homeostasis by activating the Stat2-Drp1 pathway is necessary for LPS-induced pro-inflammatory polarization in bone marrow-derived macrophages. This study found that LPS had a dual inhibitory effect on mitochondrial fusion and division in RAW264.7 cells. XBF upregulated the Mfn1 protein level. Treatment with either XBF or Mfn1 overexpression inhibited TNF-α activation and LPS-induced pro-inflammatory polarization. Our work reveals that increasing the quality, rather than the number, of mitochondrial contributes to mitigating the LPS-induced inflammatory response.

Metabolic reprogramming from OXPHOS to glycolysis is a critical feature of macrophage polarization (Saha et al., 2017). Previous studies have shown that LPS upregulates iNOS and NO expression and modifies mitochondrial complexes I and IV, thereby inhibiting OXPHOS, deletion of iNOS expression by RNAi inhibits LPS-induced pro-inflammatory polarization and enhances OXPHOS (Bailey et al., 2019). Similarly, our results have shown that LPS significantly inhibited the expression of mitochondrial complex I-V, reduced intracellular ATP levels, and increased lactic acid production. Recently, Bonnay et al. (2020) reported the role of mitochondrial fusion in promoting the capacity of OXPHOS and redistributing mtDNA between damaged and healthy mitochondria. Therefore, we hypothesized that XBF inhibits LPS-induced inflammation by regulating macrophage metabolic reprogramming. Unfortunately, there was no significant effect of XBF on mitochondrial complex expression and fatty acid oxidation, suggesting that XBF promotes mitochondrial fusion and increases the number, but not the rate, of OXPHOS. On the contrary, XBF significantly upregulated the expression of fatty acid synthase, including FASN and SREBP1. Although lipid droplets (LD) are thought to be organelles for fatty acid storage and metabolism, Bosch et al. (2020) found that several host defense proteins could be induced and assembled into complex clusters on LDs upon LPS stimulation, and different immune proteins exert synergistic antimicrobial effects through different mechanisms. Therefore, whether enhancing fatty acid synthesis and promoting LDs formation plays a role in antibacterial and antiviral effects of XBF needs to be further examined.

Conclusion

The present study demonstrates that XBF shows anti-inflammation activity in LPS-induced RAW264.7 cells and mice via inhibiting NF-κB and MAPK signaling pathways, thus suppressing pro-inflammatory polarization. Furthermore, mitochondrial biosynthesis, mitochondrial dynamics, and NLRP3 inflammasome are involved in XBF-induced inflammation inhibition in RAW264.7 cells. Our results provide a theoretical basis and biological illustration for XBF to improve patients' clinical symptoms with COVID-19.

CRediT authorship contribution statement

Zhenhao Li: Visualization, Investigation, Writing – review & editing. **Haitao Pan:** Investigation, Writing – review & editing. **Jihong Yang:** Investigation, Writing – review & editing. **Dongjie Chen:** Investigation. **Yu Wang:** Visualization. **Han Zhang:** Writing – review & editing. **Yiyu Cheng:** Visualization.

Declaration of Competing Interest

The authors declare that they have no conflict of interest.

Acknowledgments

This work was supported by the National Key Research and Development Program of China (No. 2021YFE0200300, No. 2020YFA0708000).

Supplementary materials

Supplementary material associated with this article can be found, in the online version, at doi:10.1016/j.phymed.2022.154545.

References

Andrieux, P., Chevillard, C., Cunha-Neto, E., Nunes, J.P.S., 2021. Mitochondria as a cellular hub in infection and inflammation. Int. J. Mol. Sci. 22, 11338.
Bailey, J.D., Diotallevi, M., Nicol, T., McNeill, E., Shaw, A., Chuaiphichai, S., Hale, A., Starr, A., Nandi, M., Stylianou, E., McShane, H., Davis, S., Fischer, R., Kessler, B.M., McCullagh, J., Channon, K.M., Crabtree, M.J., 2019. Nitric oxide modulates metabolic remodeling in inflammatory macrophages through TCA cycle regulation and itaconate accumulation. Cell Rep. 28, 218–230 e7.
Bonnay, F., Veloso, A., Steinmann, V., Kocher, T., Abdusselamoglu, M.D., Bajaj, S., Rivelles, E., Landskron, L., Esterbauer, H., Zinzen, R.P., Knoblich, J.A., 2020. Oxidative metabolism drives immortalization of neural stem cells during tumorigenesis. Cell 182, 1490–1507 e19.
Bosch, M., Sanchez-Alvarez, M., Fajardo, A., Kapetanovic, R., Steiner, B., Dutra, F., Moreira, L., Lopez, J.A., Campo, R., Mari, M., Morales-Paytuvi, F., Tort, O., Gubern, A., Templin, R.M., Curson, J.E.B., Martel, N., Catala, C., Lozano, F., Tebar, F., Enrich, C., Vazquez, J., Del Pozo, M.A., Sweet, M.J., Bozza, P.T., Gross, S. P., Parton, R.G., Pol, A., 2020. Mammalian lipid droplets are innate immune hubs integrating cell metabolism and host defense. Science 370.
Chan, D.C., 2020. Mitochondrial dynamics and its involvement in disease. Annu. Rev. Pathol. 15, 235–259.
Chan, J.F., Yuan, S., Kok, K.H., To, K.K., Chu, H., Yang, J., Xing, F., Liu, J., Yip, C.C., Poon, R.W., Tsoi, H.W., Lo, S.K., Chan, K.H., Poon, V.K., Chan, W.M., Ip, J.D., Cai, J. P., Cheng, V.C., Chen, H., Hui, C.K., Yuen, K.Y., 2020. A familial cluster of pneumonia associated with the 2019 novel coronavirus indicating person-to-person transmission: a study of a family cluster. Lancet 395, 514–523.
Chen, G., Wu, D., Guo, W., Cao, Y., Huang, D., Wang, H., Wang, T., Zhang, X., Chen, H., Yu, H., Zhang, X., Zhang, M., Wu, S., Song, J., Chen, T., Han, M., Li, S., Luo, X., Zhao, J., Ning, Q., 2020. Clinical and immunological features of severe and moderate coronavirus disease 2019. J. Clin. Investig. 130, 2620–2629.
Chung, K.W., Dhillon, P., Huang, S., Sheng, X., Shrestha, R., Qiu, C., Kaufman, B.A., Park, J., Pei, L., Baur, J., Palmer, M., Susztak, K., 2019. Mitochondrial damage and activation of the STING pathway lead to renal inflammation and fibrosis. Cell Metab. 30, 784–799 e5.
Coronaviridae Study Group of the International Committee on Taxonomy of, V., 2020. The species Severe acute respiratory syndrome-related coronavirus: classifying 2019-nCoV and naming it SARS-CoV-2. Nat. Microbiol. 5, 536–544.
Drozdzal, S., Rosik, J., Lechowicz, K., Machaj, F., Szostak, B., Przybycinski, J., Lorzadeh, S., Kotfis, K., Ghavami, S., Los, M.J., 2021. An update on drugs with therapeutic potential for SARS-CoV-2 (COVID-19) treatment. Drug Resist. Updat. 59, 100794.
Fang, Y., Gao, F., Hao, J., Liu, Z., 2017. microRNA-1246 mediates lipopolysaccharide-induced pulmonary endothelial cell apoptosis and acute lung injury by targeting angiotensin-converting enzyme 2. Am. J. Transl. Res. 9, 1287–1296.
Fontecha-Barriuso, M., Martin-Sanchez, D., Martinez-Moreno, J.M., Carrasco, S., Ruiz-Andres, O., Monsalve, M., Sanchez-Ramos, C., Gomez, M.J., Ruiz-Ortega, M., Sanchez-Nino, M.D., Cannata-Ortiz, P., Cabello, R., Gonzalez-Enguita, C., Ortiz, A., Sanz, A.B., 2019. PGC-1alpha deficiency causes spontaneous kidney inflammation and increases the severity of nephrotoxic AKI. J. Pathol. 249, 65–78.
Galluzzi, L., Kepp, O., Kroemer, G., 2012. Mitochondria: master regulators of danger signalling. Nat. Rev. Mol. Cell Biol. 13, 780–788.
Geto, Z., Molla, M.D., Challa, F., Belay, Y., Getahun, T., 2020. Mitochondrial dynamic dysfunction as a main triggering factor for inflammation associated chronic non-communicable diseases. J. Inflamm. Res. 13, 97–107.
Grant, R.A., Morales-Nebreda, L., Markov, N.S., Swaminathan, S., Querrey, M., Guzman, E.R., Abbott, D.A., Donnelly, H.K., Donayre, A., Goldberg, I.A., Klug, Z.M., Borkowski, N., Lu, Z., Kihshen, H., Politanska, Y., Sichizya, L., Kang, M., Shilatifard, A., Qi, C., Lomasney, J.W., Argento, A.C., Kruser, J.M., Malsin, E.S., Pickens, C.O., Smith, S.B., Walter, J.M., Pawlowski, A.E., Schneider, D., Nannapaneni, P., Abdala-Valencia, H., Bharat, A., Gottardi, C.J., Budinger, G.R.S., Misharin, A.V., Singer, B.D., Wunderink, R.G., Investigators, N.S.S., 2021. Circuits between infected macrophages and T cells in SARS-CoV-2 pneumonia. Nature 590, 635–641.
Halling, J.F., Pilegaard, H., 2020. PGC-1alpha-mediated regulation of mitochondrial function and physiological implications. Appl. Physiol. Nutr. Metab. 45, 927–936.
Jehn, U., Bayraktar, S., Pollmann, S., Van Marck, V., Weide, T., Pavenstadt, H., Brand, E., Lenders, M., 2021. alpha-galactosidase a deficiency in fabry disease leads to extensive dysregulated cellular signaling pathways in human podocytes. Int. J. Mol. Sci. 22, 11339.
Jose, R.J., Manuel, A., 2020. COVID-19 cytokine storm: the interplay between inflammation and coagulation. Lancet Respir. Med. 8, e46–e47.
Karki, R., Sharma, B.R., Tuladhar, S., Williams, E.P., Zalduondo, L., Samir, P., Zheng, M., Sundaram, B., Banoth, B., Malireddi, R.K.S., Schreiner, P., Neale, G., Vogel, P., Webby, R., Jonsson, C.B., Kanneganti, T.D., 2021. Synergism of TNF-alpha and IFN-

gamma triggers inflammatory cell death, tissue damage, and mortality in SARS-CoV-2 infection and cytokine shock syndromes. Cell 184, 149–168 e17.
Kayagaki, N., Warming, S., Lamkanfi, M., Vande Walle, L., Louie, S., Dong, J., Newton, K., Qu, Y., Liu, J., Heldens, S., Zhang, J., Lee, W.P., Roose-Girma, M., Dixit, V.M., 2011. Non-canonical inflammasome activation targets caspase-11. Nature 479, 117–121.
Kumar, V., 2020. Pulmonary innate immune response determines the outcome of inflammation during pneumonia and sepsis-associated acute lung injury. Front. Immunol. 11, 1722.
LaVergne, S.M., Stromberg, S., Baxter, B.A., Webb, T.L., Dutt, T.S., Berry, K., Tipton, M., Haberman, J., Massey, B.R., McFann, K., Alnachoukati, O., Zier, L., Heacock, T., Ebel, G.D., Henao-Tamayo, M., Dunn, J., Ryan, E.P., 2021. A longitudinal SARS-CoV-2 biorepository for COVID-19 survivors with and without post-acute sequelae. BMC Infect. Dis. 21, 677.
Li, A., Yang, J., Qian, J., Shao, X., Liao, J., Lu, X., Fan, X., 2022. Tracing the cell-type-specific modules of immune responses during COVID-19 progression using scDisProcema. Comput. Struct. Biotechnol. J. 20, 3545–3555.
Li, P., Hu, S., Qian, C., Yao, Y., Li, L.Y., Yang, J.F., Yang, L., Yang, C.C., Zhou, H., Wang, S.X., Hu, Y., Zhu, X.Y., Zhou, J., Pan, L.X., Shen, C.P., Zhou, H., 2021a. The therapeutic effect of traditional chinese medicine on inflammatory diseases caused by virus, especially on those caused by COVID-19. Front. Pharmacol. 12, 650425.
Li, Y., Li, B., Wang, P., Wang, Q., 2021b. Traditional Chinese medicine, Qingfei Paidu decoction and Xuanfei Baidu decoction, inhibited cytokine production via NF-kappaB signaling pathway in macrophages: implications for coronavirus disease 2019 (COVID-19) therapy. Front. Pharmacol. 12, 722126.
Liu, F., Qiu, H., Xue, M., Zhang, S., Zhang, X., Xu, J., Chen, J., Yang, Y., Xie, J., 2019. MSC-secreted TGF-beta regulates lipopolysaccharide-stimulated macrophage M2-like polarization via the Akt/FoxO1 pathway. Stem Cell Res. Ther. 10, 345.
Liu, L., Guo, H., Song, A., Huang, J., Zhang, Y., Jin, S., Li, S., Zhang, L., Yang, C., Yang, P., 2020. Progranulin inhibits LPS-induced macrophage M1 polarization via NF-small ka, CyrillicB and MAPK pathways. BMC Immunol. 21, 32.
Liu, Q., Zhang, D., Hu, D., Zhou, X., Zhou, Y., 2018. The role of mitochondria in NLRP3 inflammasome activation. Mol. Immunol. 103, 115–124.
Liu, Y.C., Zou, X.B., Chai, Y.F., Yao, Y.M., 2014. Macrophage polarization in inflammatory diseases. Int. J. Biol. Sci. 10, 520–529.
Lv, J., Wang, Z., Qu, Y., Zhu, H., Zhu, Q., Tong, W., Bao, L., Lv, Q., Cong, J., Li, D., Deng, W., Yu, P., Song, J., Tong, W.M., Liu, J., Liu, Y., Qin, C., Huang, B., 2021. Distinct uptake, amplification, and release of SARS-CoV-2 by M1 and M2 alveolar macrophages. Cell Discov. 7, 24.
Lyu, M., Fan, G., Xiao, G., Wang, T., Xu, D., Gao, J., Ge, S., Li, Q., Ma, Y., Zhang, H., Wang, J., Cui, Y., Zhang, J., Zhu, Y., Zhang, B., 2021. Traditional Chinese medicine in COVID-19. Acta Pharm. Sin. B 11, 3337–3363.
Man, S.M., Karki, R., Kanneganti, T.D., 2017. Molecular mechanisms and functions of pyroptosis, inflammatory caspases and inflammasomes in infectious diseases. Immunol. Rev. 277, 61–75.
Meyer, A., Laverny, G., Bernardi, L., Charles, A.L., Alsaleh, G., Pottecher, J., Sibilia, J., Geny, B., 2018. Mitochondria: an organelle of bacterial origin controlling inflammation. Front. Immunol. 9, 536.
Musa, H.H., Musa, T.H., Musa, I.H., Musa, I.H., Ranciaro, A., Campbell, M.C., 2021. Addressing Africa's pandemic puzzle: Perspectives on COVID-19 transmission and mortality in sub-Saharan Africa. Int. J. Infect. Dis. 102, 483–488.
Na, K., Li, K., Sang, T., Wu, K., Wang, Y., Wang, X., 2017. Anticarcinogenic effects of water extract of sporoderm-broken spores of Ganoderma lucidum on colorectal cancer *in vitro* and *in vivo*. Int. J. Oncol. 50, 1541–1554.
Otera, H., Ishihara, N., Mihara, K., 2013. New insights into the function and regulation of mitochondrial fission. Biochim. Biophys. Acta 1833, 1256–1268.
Pan, X., Dong, L., Yang, L., Chen, D., Peng, C., 2020. Potential drugs for the treatment of the novel coronavirus pneumonia (COVID-19) in China. Virus Res. 286, 198057.
Pastva, A., Estell, K., Schoeb, T.R., Atkinson, T.P., Schwiebert, L.M., 2004. Aerobic exercise attenuates airway inflammatory responses in a mouse model of atopic asthma. J. Immunol. 172, 4520–4526.
Ross, E.A., Devitt, A., Johnson, J.R., 2021. Macrophages: the good, the bad, and the gluttony. Front. Immunol. 12, 708186.
Rowe, G.C., Raghuram, S., Jang, C., Nagy, J.A., Patten, I.S., Goyal, A., Chan, M.C., Liu, L. X., Jiang, A., Spokes, K.C., Beeler, D., Dvorak, H., Aird, W.C., Arany, Z., 2014. PGC-1alpha induces SPP1 to activate macrophages and orchestrate functional angiogenesis in skeletal muscle. Circ. Res. 115, 504–517.
Saha, S., Shalova, I.N., Biswas, S.K., 2017. Metabolic regulation of macrophage phenotype and function. Immunol. Rev. 280, 102–111.
Saki, M., Prakash, A., 2017. DNA damage related crosstalk between the nucleus and mitochondria. Free Radic. Biol. Med. 107, 216–227.
Sefik, E., Qu, R., Junqueira, C., Kaffe, E., Mirza, H., Zhao, J., Brewer, J.R., Han, A., Steach, H.R., Israelow, B., Blackburn, H.N., Velazquez, S., Chen, Y.G., Halene, S., Iwasaki, A., Meffre, E., Nussenzweig, M., Lieberman, J., Wilen, C.B., Kluger, Y., Flavell, R.A., 2022. Inflammasome activation in infected macrophages drives COVID-19 pathology. Nature 606, 585–593.
Shih, P.H., Shiue, S.J., Chen, C.N., Cheng, S.W., Lin, H.Y., Wu, L.W., Wu, M.S., 2021. Fucoidan and fucoxanthin attenuate hepatic steatosis and inflammation of NAFLD through modulation of leptin/adiponectin axis. Mar. Drugs 19, 148.
Sica, A., Erreni, M., Allavena, P., Porta, C., 2015. Macrophage polarization in pathology. Cell. Mol. Life Sci. 72, 4111–4126.
Viola, A., Munari, F., Sanchez-Rodriguez, R., Scolaro, T., Castegna, A., 2019. The metabolic signature of macrophage responses. Front. Immunol. 10, 1462.
Wang, D., Hu, B., Hu, C., Zhu, F., Liu, X., Zhang, J., Wang, B., Xiang, H., Cheng, Z., Xiong, Y., Zhao, Y., Li, Y., Wang, X., Peng, Z., 2020a. Clinical characteristics of 138 hospitalized patients with 2019 novel coronavirus-infected pneumonia in Wuhan, China. JAMA 323, 1061–1069.
Wang, X., Quan, S., Zhang, H., Song, X., Zhang, J., Liu, D., 2022a. Development and validation of a sensitive UPLC-Q-TOF-MS/MS for the measurement of nine components in rat plasma and tissues and its application to pharmacokinetics and tissue distribution studies with Xuanfei Baidu granules. Curr. Drug Metab. 23, 150–163.
Wang, Y., Li, X., Zhang, J.H., Xue, R., Qian, J.Y., Zhang, X.H., Zhang, H., Liu, Q.Q., Fan, X.H., Cheng, Y.Y., Zhang, B.L., 2020b. [Mechanism of Xuanfei Baidu Tang in treatment of COVID-19 based on network pharmacology]. Zhongguo Zhong Yao Za Zhi 45, 2249–2256.
Wang, Y., Wang, X., Li, Y., Xue, Z., Shao, R., Li, L., Zhu, Y., Zhang, H., Yang, J., 2022b. Xuanfei Baidu decoction reduces acute lung injury by regulating infiltration of neutrophils and macrophages via PD-1/IL17A pathway. Pharmacol. Res. 176, 106083.
Wang, Z., Yang, L., 2021. Chinese herbal medicine: fighting SARS-CoV-2 infection on all fronts. J. Ethnopharmacol. 270, 113869.
Xian, H., Liu, Y., Rundberg Nilsson, A., Gatchalian, R., Crother, T.R., Tourtellotte, W.G., Zhang, Y., Aleman-Muench, G.R., Lewis, G., Chen, W., Kang, S., Luevanos, M., Trudler, D., Lipton, S.A., Soroosh, P., Teijaro, J., de la Torre, J.C., Arditi, M., Karin, M., Sanchez-Lopez, E., 2021. Metformin inhibition of mitochondrial ATP and DNA synthesis abrogates NLRP3 inflammasome activation and pulmonary inflammation. Immunity 54, 1463–1477 e11.
Xiong, W.Z., Wang, G., Du, J., Ai, W., 2020. Efficacy of herbal medicine (Xuanfei Baidu decoction) combined with conventional drug in treating COVID-19: a pilot randomized clinical trial. Integr. Med. Res. 9, 100489.
Yang, Y., Jiang, G., Zhang, P., Fan, J., 2015. Programmed cell death and its role in inflammation. Mil. Med. Res. 2, 12.
Yu, W., Wang, X., Zhao, J., Liu, R., Liu, J., Wang, Z., Peng, J., Wu, H., Zhang, X., Long, Z., Kong, D., Li, W., Hai, C., 2020. Stat2-Drp1 mediated mitochondrial mass increase is necessary for pro-inflammatory differentiation of macrophages. Redox. Biol. 37, 101761.
Zhao, J., Guo, D., Fan, M., Liu, Y., 2021a. Efficacy and safety of Xuanfei Baidu granules for treating COVID-19: a protocol for systematic review and meta-analysis. Medicine (Baltimore) 100, e25653.
Zhao, L., Liu, H., Wang, Y., Wang, S., Xun, D., Wang, Y., Cheng, Y., Zhang, B., 2021b. Multimodal Identification by transcriptomics and multiscale bioassays of active components in Xuanfeibaidu formula to suppress macrophage-mediated immune response. Engineering. Beijing.
Zhong, Z., Liang, S., Sanchez-Lopez, E., He, F., Shalapour, S., Lin, X.J., Wong, J., Ding, S., Seki, E., Schnabl, B., Hevener, A.L., Greenberg, H.B., Kisseleva, T., Karin, M., 2018. New mitochondrial DNA synthesis enables NLRP3 inflammasome activation. Nature 560, 198–203.